Synthesis, structure and catalytic promiscuity of a napthyl-pyrazole Mn(II) complex and structure–activity relationships

Abhimanyu Jana, Paula Brandão, Harekrishna Jana, Atish Dipankar Jana, Gopinath Mondal, Pradip Bera, Ananyakumari Santra, Ajit Kumar Mahapatra & Pulakesh Bera

Check for updates

Synthesis, structure and catalytic promiscuity of a napthyl-pyrazole Mn(II) complex and structure–activity relationships

Abhimanyu Jana[a], Paula Brandão[b] (iD), Harekrishna Jana[c], Atish Dipankar Jana[d], Gopinath Mondal[a], Pradip Bera[a,e], Ananyakumari Santra[a], Ajit Kumar Mahapatra[f] and Pulakesh Bera[a] (iD)

[a]Post Graduate Department of Chemistry, Panskura Banamali College (Vidyasagar University), Midnapore (East), India; [b]Department of Chemistry, CICECO, University of Aveiro, Aveiro, Portugal; [c]Department of Microbiology, Panskura Banamali College (Vidyasagar University), Midnapore (East), India; [d]Department of Physics, Behala College, Kolkata, India; [e]Department of Chemistry, Kandi Raj College, Murshidabad, India; [f]Department of Chemistry, Indian Institute of Engineering Science and Technology, Howrah, India

ABSTRACT

The napthyl/pyridine-pyrazole-derived complexes, $[Mn(L^1)Cl_2]$ (**1**), $[Co(L^1)Cl_2]$ (**2**), $[Cu(\mu-Cl)(Cl)(L)]_2$ (**3**), $[Cu_2(L)_2(N_3)_3(\mu2-N_3)]$ (**4**), and $[Co(L^2)Cl_2]$ (**5**) (where L^1 = bis-(3,5-dimethyl-pyrazol-1-ylmethyl)-napthalen-1-ylmethyl-amine (L^1), L = 5-methyl-pyrazol-1-ylmethyl)-napthalen-1-ylmethyl-amine (L) and L^2 = 2-[2-(3,5-dimethyl-pyrazol-1-yl)-1-methyl-ethyl]-pyridine), exhibited phenoxazinone synthase activity in methanol in the range $5–54 h^{-1}$. Binuclear copper(II) derivatives **3** and **4** show better catalytic activities than manganese(II) and cobalt(II) derivatives. The kinetic studies reveal that phenoxazinone chromophore is produced *via* a complex-substrate intermediate. Further, **3** and **4** show catecholase activity in methanol in the presence of oxygen. All the complexes showed potent antimicrobial activity against the tested strains of bacteria and fungi. Complex **1** was synthesized for the first time by mixing L^1 and $MnCl_2$ (1:1) and characterized by single-crystal X-ray crystallography, cyclic voltammetry, density functional theory, and thermogravimetry analysis. The present study suggests that napthyl/pyridyl-anchored pyrazole metal complexes are interesting scaffolds for the development of novel model compounds for biochemical reaction and efficient antimicrobial agents.

CONTACT Pulakesh Bera ✉ pbera.pbc.chem@gmail.com ▣ Post Graduate Department of Chemistry, Panskura Banamali College (Vidyasagar University), Panskura R.S., Midnapore (East), West Bengal 721152, India.
ⓘ Supplemental data for this article is available online at https://doi.org/10.1080/00958972.2019.1658192.
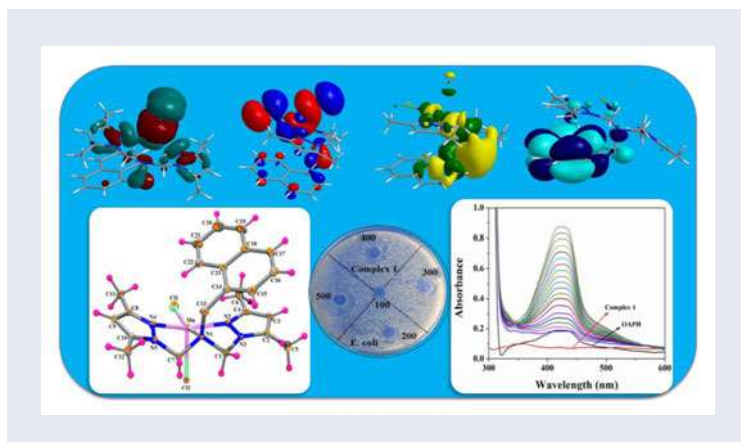
1. Introduction

Pyrazole (1,2-diazole) which is isomeric to imidazole (1,3-diazole), an integral part of histidine unit of several proteins, has great interest due to its wide range of applications in catalysis, medicine, and agro-chemicals [1–4]. The attractiveness of pyrazole and its derivatives is their versatility that allows for the synthesis of a series of analog building blocks with different moieties which affect the electronic properties of the resultant compounds [5]. Biological applications of pyrazole derivatives such as antifungal, antitubercular, antibacterial, antiviral [6–8], antioxidant [1, 9–11], anti-inflammatory [12], antipyretic, antimicrobial [13], anticonvulsant [14], antihistaminic [15], antidepressant [16], insecticides, and fungicides [17] were well documented.

The event of biocatalysts and catalytic promiscuity has been focused by bioinorganic chemists in recent years [18–20]. Generally, enzymes have high efficiency and specificity but in many cases, a single catalytic site can activate more than one biochemical transformation. This phenomenon is known as catalytic promiscuity. The literature on biomimetic studies has shown several examples of such catalytic promiscuity over the last two decades [21]. Attempts have been made for modeling the active site of several metalloenzymes like hydrolase, phosphodiesterase, superoxide dismutase (SOD), nuclease, phenoxazinone synthase (PHS), and catecholase oxidase (CO) activities with rationally synthesized model complexes [22]. The enzyme-donor sites are rationally designed with small molecule ligands which are then incorporated with metals to form metal complexes. Generally, Cu^{II}/Cu^{I}, Co^{III}/Co^{II}, Ni^{II}, Fe^{II}/Fe^{III}, Mn^{II}, and Zn^{II} ions are used for bio-mimetic functional models and mechanistic studies [23]. It has been noticed that the strongly coordinated multiple N-donors enhance the rate of enzymatic reaction [23]. Several multiple N-donors and N,O-donors are modeled for enzymatic study. Several pyrazole-derived multipodal copper(II) complexes showing CO activity were reported [24, 25]. Earlier, Malachowski and Davison reported CO activity of some pyrazole-derived ligands [26]. In view of potential biological activity of pyrazolyl derivatives, we explore the various pyrazole-based compounds annexed with napthalene/pyridine for biomimicking activities. Herein, we

report the PHS activity of **1–5** and CO mimicking activities of **3** and **4** with detailed kinetic studies. The antimicrobial activities of the napthyl/pyridyl-pyrazole derivatives **1–5** have been screened with eight bacteria, *Escherichia coli*, *Staphylococcus aureus*, *Streptococcus faecalis*, *Salmonella typhi*, *Proteus vulgaris*, *Pseudomonas aeruginosa*, *Klebsiella pneumonia*, and *Bacillus subtilis*, and two fungi *Aspergillus flavus* and *Candida albicans*. The synthesis and structural characterization of **1** is reported for the first time.

2. Experimental

2.1. Materials and reagents

The starting materials for the synthesis of the ligands like acetylacetone, hydrazine hydrate, formalin, 2-methylamino-pyridine, 1-methyl-napthyl-amine, 2-amino-phenol, and 3,5-ditertiary-butyl-catechol were purchased from Aldrich Chemical Company and used as procured. Copper(II) chloride dihydrate, copper(II) nitrate hexahydrate, manganese(II) chloride trihydrate, cobalt(II) chloride hexahydrate, and sodium azide were purchased from Merck, India, and used for the preparation of complexes. Solvents like methanol, ethanol, chloroform, diethyl ether, and acetonitrile were of reagent grade and dried before use.

2.1.1. Synthesis of ligands

The present ligands were synthesized by the condensation of 3,5-dimethyl-pyrazole-1-carbinol and amine at ambient conditions. The preparation of 3,5-dimethyl-pyrazole-1-carbinol is carried out following a known literature procedure [26, 27]. The details of L^1 and L^2 preparation and characterization were reported earlier by one of the authors (A Jana) [28].

2.1.2. Preparation of [Mn(L^1)Cl$_2$] (1)

$MnCl_2 \cdot 3H_2O$ (1 mmol, 0.241 g) was added to a solution of L^1 (1 mmol, 0.373 g) in 20-mL acetonitrile at room temperature. The mixture was stirred for 0.5 h. The resultant solid was filtered off and dried over silica gel. Colorless crystals suitable for X-ray crystallography were obtained from the acetonitrile solution of L^1. Yield: 62% (based on metal salt). CHN Analysis found (calcd) for $C_{23}H_{27}Cl_2MnN_5$: C, 55.31 (55.27); H, 5.37 (5.40); N, 13.96 (14.01). IR assignments (KBr pellet) (in cm^{-1}); $\nu(C=C)_{pyrazole}$ 1571 (strong(s)); $\nu(C=N)_{pyrazole}$ 1465 (s); $\nu(C-N)_{aliphatic\ amine}$ 1304 (s).

Complexes **2–5** were synthesized once again following the procedures [28, 29] to investigate and compare their catalytic efficiency with **1**. The isolation of **3** and **4** was obtained prior to dissociation of L^1, where one pyrazole unit was lost during complexation. The details of the fragmentation of L^1 and the formation of **3** and **5** were described earlier and are not included in the present study. We recrystallized **1–5**, L^1 and L^2 before *in vitro* biological experiments.

2.2. Physical measurements

Elemental analysis (C, H, and N) were carried out using a FISONS EA-1108 CHN analyzer. The FTIR analyses were performed by using a Perkin Elmer Spectrum Two Spectrophotometer (400–4000 cm^{-1}). The samples were prepared as KBr pellets using anhydrous KBr salt. The UV-vis spectra of the complex were measured using a Perkin Elmer Lamda-35 spectrophotometer with a 1-cm path length quartz-cell. TGA analysis of **1** is performed using an instrument from Perkin Elmer, model TGA 4000, at a heating rate of 20 °C/min under nitrogen. The ground-state electronic structure calculations have been carried out using the X-ray coordinates of the complex with the help of DFT [30] methods with the Orca 2.7 program [31]. Becke's hybrid function [30] with the Lee-Yang-Parr (LYP) correlation function [32] was used throughout the study. LANL2DZ valence and effective core potential functions were used. All energy calculations were performed using the self-consistent field "tight" option of the Orca 2.7 program to ensure sufficiently well-converged values for the state energies. Cyclic voltammetry studies were performed at room temperature in methanol solvent using tetrabutylammonium perchlorate as a supporting electrolyte on a CH Instrument electrochemical workstation model no CHI630E. The conventional three-electrode assembly is comprised of a platinum working electrode, a platinum wire auxiliary electrode, and Ag/AgCl reference electrode.

2.3. X-ray crystallography

The single-crystal X-ray diffraction (XRD) of **1** was carried out on a Bruker SMART APEX II X-ray diffractometer equipped with graphite-monochromated Mo-Kα radiation (λ = 0.71073 Å) and 16 CCD area detector. The intensity data were collected in the π and ω scan mode, operating at 50 kV, 30 mA at 296 K [33]. The data reduction was performed using SAINT and SADABS [34]. All calculations in the structural solution and refinement were performed using the Bruker SHELXTL program [35]. The structure was solved by the heavy atom method and refined by full-matrix least-squares methods. All the non-hydrogen atoms were refined anisotropically; hydrogens were geometrically positioned and fixed with isotropic thermal parameters. The final electron density maps showed no significant difference.

2.4. Kinetics of catalytic activity

The PHS mimicking activity of **1–5** was studied by monitoring the oxidation of O-aminophenol (OAPH) spectrophotometrically in dioxygenated methanol at 25 °C. Auto-oxidation of substrate is strictly prohibited by not adding any base. All the complexes in the concentration 1×10^{-5} M catalyze the formation of phenoxazinone from OAPH in oxygenated methanol showing progressive increase of peak intensity at 435 nm, which is characteristic of phenoxazinone chromophore. It is to be noted that blank experiment without complex (catalyst) does not give any peak at 435 nm in an identical reaction condition. To examine the catalyst dependency on the rate of the reaction, the amounts of the catalyst (10–200 $\times 10^{-5}$ M) were mixed with a fixed concentration of substrate (1×10^{-3} M) in methanol (2.0 mL) saturated with dioxygen. Same

concentration of substrate and catalysts (**3** and **4**) was also maintained for catecholase activity and kinetic study.

2.5. Determination of the logP by using the shake-flask method

Lipophilicity of the ligands and complexes are determined by calculating *logP* values according to the shake-flask method [36]. Compounds under investigation were weighted out accurately and partitioned between equal volumes of water and 1-octanol (5 mL each) by shaking for 30 h at room temperature to assure full partitioning of the analyzed compounds between two water and 1-octanol phases. Then, the solution was centrifuged at 3500 rpm for 10 min to separate two layers. The concentration of the compounds in different layers was measured by the optical density values obtained from UV-Vis spectroscopy.

2.6. Antibacterial assays

Antibacterial sensitivity of the five metal complexes along with free L^1 and L^2 was tested by the agar well diffusion method using Mueller–Hilton agar media. The agar diffusion method was employed for the determination of antibacterial activities according to the method described by van den Berghe and Vlietinck in 1991 [37]. The compounds under investigation were dissolved in methanol and acetonitrile to a final concentration of 1000 μg/mL. Eight species of pathogenic bacteria, *Escherichia coli*, *Staphylococcus aureus*, *Streptococcus faecalis*, *Salmonella typhi*, *Proteus vulgaris*, *Klebsiella pneumonia*, *Pseudomonas aeruginosa,* and *Bacillus subtilis*, were used to screen the antibacterial activity of the metal complex [38]. Pathogenic bacterial strains were incubated in sterile nutrient broth and incubated at 37 °C for 24 h. The pathogens were swabbed (inoculum size was adjusted so as to deliver a final inoculums of approximately 10^6 CFU/mL) on the surface of Mueller–Hilton agar media and petri dishes containing 20 mL of Mueller–Hinton agar with 100 μL inoculums of bacterial strain and media were allowed to solidify. Wells were cut into solidified agar media with the help of sterilized cup-borer; 100 μL of each sample solution was poured in the respective wells and the plates including control were incubated overnight at 37 °C for bacteria. The experiment was performed in triplicate under strict aseptic conditions and the antibacterial activity of each compound was expressed in terms of the mean diameter of zone of inhibition (cm) produced by the respective compound.

Similarly, antifungal sensitivity is tested by the agar well diffusion method using PD agar media [38]. Two species of pathogenic fungi, *Aspergillus flavus* and *Candida albicans*, are used to screen the antifungal activity of the pyrazolyl compounds. Pathogenic fungal strain is inoculated in sterile potato dextrose broth and incubated at 25 °C for 48–72 h. Petri dishes containing 25 mL of potato dextrose agar with 100 μL inoculums of fungal strain and media are allowed to solidify. The remaining work-up process is similar to that of antibacterial sensitivity test. The stock solution (5000 μg/mL) was made by dissolving the antibiotic in sterile distilled water. From this stock solution, 1000 μg/mL was prepared for determination of the sensitivity of fungi.
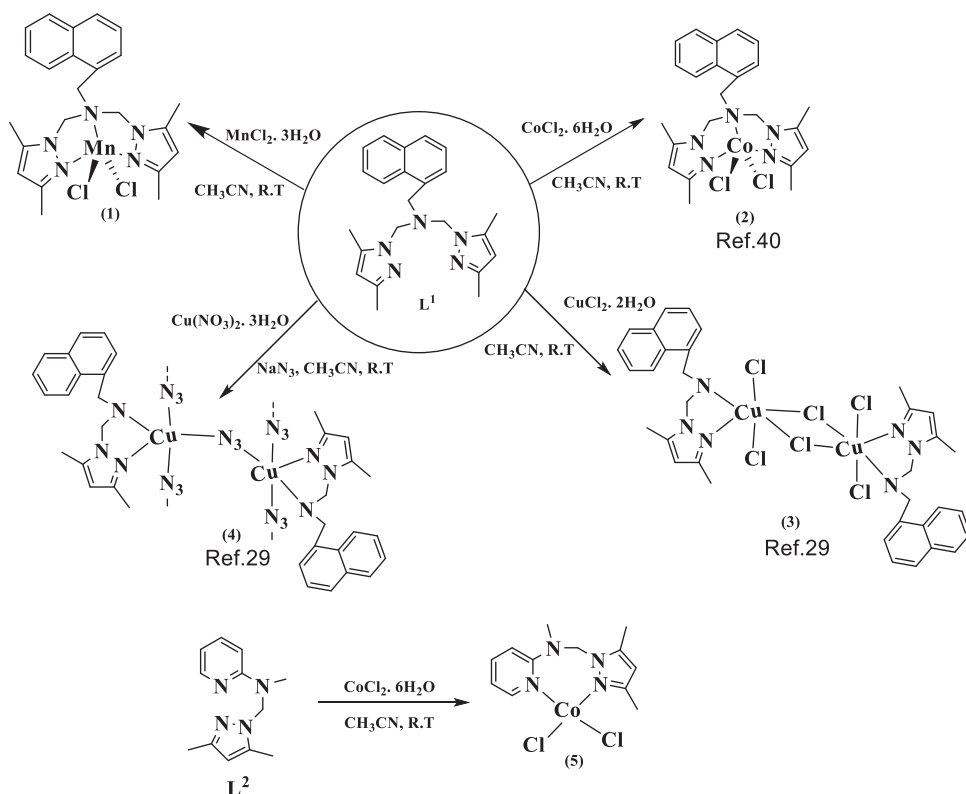
Scheme 1. Schematic presentation of preparation of **1–5** with L^1 and L^2.

2.7. Determination of MIC value

Minimum inhibitory concentration (MIC) was determined using inhibitory concentration in diffusion (ICD) method [23]. The MIC values, which represent the lowest concentration of the compound that completely inhibits the growth of microorganisms, were determined by a micro-well dilution method [24]. The inoculums of each bacterium were prepared and the suspensions were adjusted to 10^6 CFU/mL. For making these dilutions, metal complexes were dissolved at a required concentrations and diluted with methanol to obtain concentration 1000 μg/mL, 800 μg/mL, 600 μg/mL, 400 μg/mL, 200 μg/mL and 100 μg/mL in the respective wells and the plates were incubated for 24 h at 37 °C. The experiment was performed in triplicate under strict aseptic conditions.

3. Results and discussion

3.1. Chemistry

Primarily dioxygen activation and oxygenation occur at the active site(s) of an enzyme in the process of phenoxazinone and quinone synthesis. This fundamental idea should be considered in designing mimics of metallo-enzymes. The present work includes two pyrazole-based ligands, L^1 and L^2, with varying substitutions in pyrazolyl-
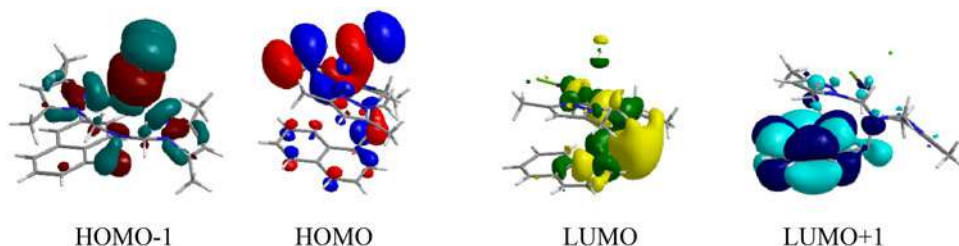
Figure 1. Surface plots of 1.

methylamine with napthalene and pyridine group, respectively. Anchoring with napthyl/pyridyl group with pyrazole-core unit eventually increases steric crowding in the resultant molecules (Scheme 1). To relieve the steric repulsion, L¹ dissociates before the formation of 3 and 4 as explained earlier by us [27]. However, L¹ forms stable mononuclear complexes of manganese(II) (1) and cobalt(II) (2) with undissociated ligand form (Supplementary Figures S3 and S4) [39]. The reasons are by no means certain but several factors are involved. The size of the ligand is probably a major one. Fragmented L¹ less by one methylpyrazole unit prefers to stabilize the bridged copper(II) complex rather than a mononuclear Cu(II)–L¹ complex. There is a delicate balance between the formation of chelate with undissociated ligand and the formation of polynuclear chain with dissociated fragment [29, 40]. The inherent electronic as well as steric factors of the ligands and their metal complexes bearing pyrazolyl-scaffold might be potential showing biological functions. The chemistry and details of characterization of complexes, except 1, are reported earlier by us [28].

3.2. Structural characterization of 1

FTIR characterization is done comparing the spectrum of 1 and that of L¹ (Supplementary Figure S1). The peaks in the spectrum of complexes are less in number and quite sharper than the spectrum of L¹, clearly providing strong binding of ligand with Mn(II) ion. The presence of a strong band at 1548 cm⁻¹ for L¹ due to $\nu(C=N)$ is shifted to lower frequency at 1465 cm⁻¹ in 1, indicating the involvement of tertiary N atom in coordination with manganese atom. The positive shift of $\nu(N-N)_{pz}$ at 1240 cm⁻¹ for L¹ to 64 cm⁻¹ on complexation with Mn(II) indicates the involvement of pyrazolyl tertiary N atom in bonding.

Analysis of single-point DFT of 1 reveals the contribution of chloride ions in HOMO and HOMO−1 function where the pyrazole and napthalene moieties contribute more in the formation of LUMO and LUMO + 1 function (Figure 1). These theoretical data suggest that the complex is labile with respect to chloride substitution.

Thermal decomposition of 1 has been performed to study the decomposition pattern of the complex (Figure 2 and Scheme 2). The decomposition of 1 occurs in four steps. The first step of decomposition of 1 starts at 80 °C and continues up to 150 °C, giving a sharp loss of 33.46% of total mass. This mass loss can be assigned to the loss of 1-methyl napthylamine group (ca. 31.16%). The second step of decomposition accounts for 5.6% of the total mass which referred to the loss of two CH₂ units attached to the N atom of pyrazole. About 14.3% weight loss occurred in the third
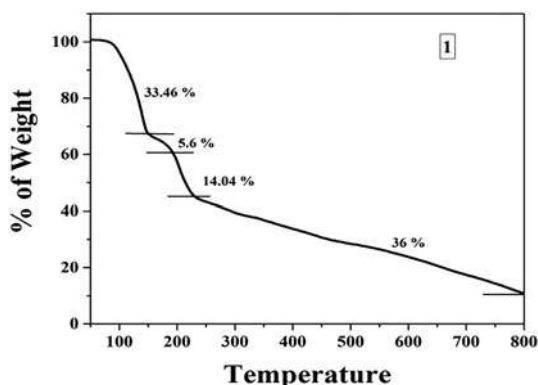
Figure 2. TG of **1** in nitrogen atmosphere with sample of amount 1 mg at a heating rate 10 °C/min.
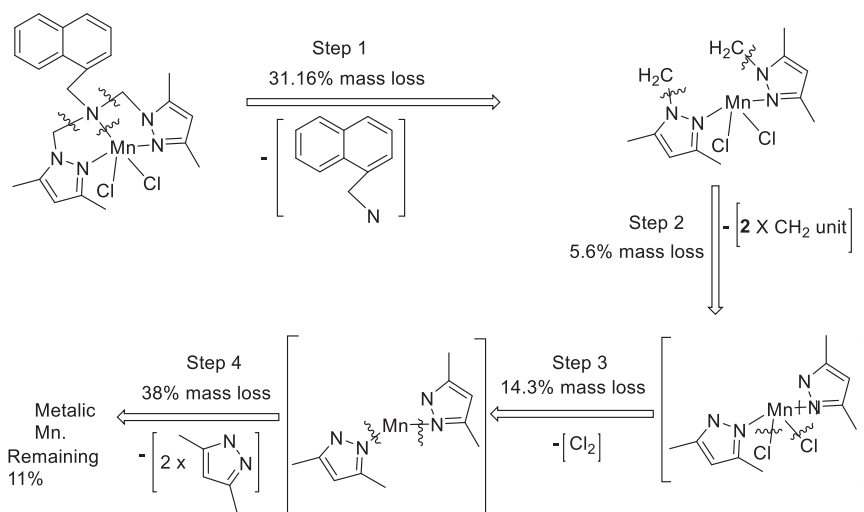
Scheme 2. Plausible mechanism of decomposition of **1**.

step of decomposition of **1** at 180–240 °C, which can be attributed to the loss of coordinated chlorine as $Cl_{2(g)}$. At the fourth step of decomposition, weight loss of 38% occurred due to the loss of two 3,5-dimethylpyrazolyl units. The last step of decomposition (estimated 8%) comprises the loss of remaining organics from 210 to 800 °C, giving residual metallic manganese (i.e. 11%).

3.3. X-ray crystallography of 1

The molecular structure of **1** consists of one tridentate N,N,N-donor ligand L^1 with two chlorido ligands, resulting in a five-coordinate manganese(II) center with the MnN_3Cl_2 chromophore. The geometry of the five-coordinate metal center can be ascertained by the Addison parameter (τ) [41]. The τ value is 0.38 for **1** (τ = (α − β)/60, where α and β are the two largest ligand-metal-ligand angles of the coordination sphere), suggesting a distorted square pyramid (τ = 0 for a perfect square pyramid and τ = 1 for a
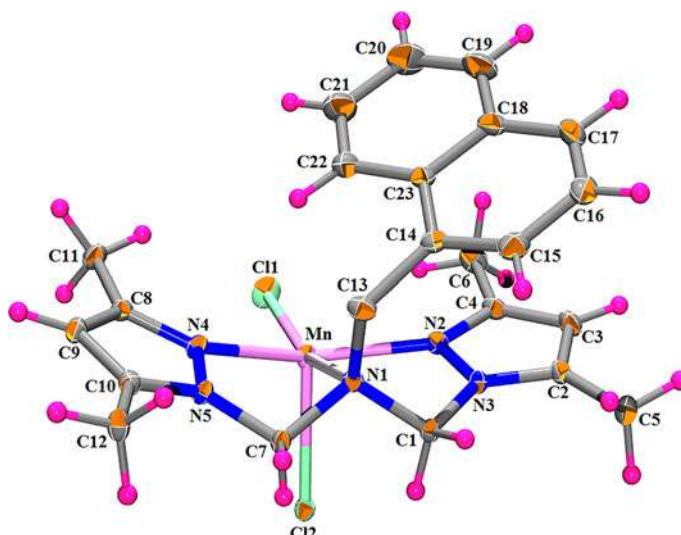
Figure 3. ORTEP diagram (30% ellipsoidal probability) with atom numbering scheme of **1**.

Table 1. Crystal data and refinement parameters of the structure of 1.

Crystal data	
Formula	$C_{23}H_{27}Cl_2MnN_5$
Formula weight	499.34
CCDC No.	1865481
Crystal system	Orthorhombic
Space group	P2₁2₁2₁ (No. 19)
a, b, c [Å]	8.5764(3), 10.3057(4), 26.5632(10)
V [Å³]	2347.81(15)
Z	4
D(calc) [g/cm³]	1.413
μ(MoKα) [/mm]	0.810
F(000)	1036
Crystal size [mm]	$0.10 \times 0.20 \times 0.30$
Data collection	
Temperature (K)	150
Radiation [Å] MoKα	0.71073
θ_min-max [Deg]	1.5, 29.2
Data set	−11: 10; −14: 9; −36: 36
Tot., Uniq. data, R(int)	22803, 6212, 0.039
Observed data [I > 2.0 σ(I)]	5293
Refinement	
Nref, Npar	6212, 284
R, wR2, S	0.0341, 0.0696, 1.02
Max. and av. shift/error	0.00, 0.00
Flack x	0.025(9)
Min. and max. resd. dens. [e/Å³]	−0.26, 0.25

$w = \frac{1}{[\sigma^2(F_0^2)+(0.0267P)^2+0.2598P]}$ where $P = (F_0^2 + 2F_C^2)/3$.

perfect trigonal bipyramid). The ORTEP diagram of [MnL¹Cl₂] (**1**) is given in Figure 3. Complex **1** crystallized in the orthorhombic system with space group P2₁2₁2₁ with manganese in +2 oxidation state. The Mn–N bonds are shorter than Mn–Cl bonds, Mn–N2 = 2.171 Å, Mn–N4 = 2.198 Å, Mn–Cl1 = 2.3443 Å, and Mn–Cl2 = 2.4076 Å, except for the tertiary-N atom where Mn–N1 = 2.572 Å. The long bond Mn-N1 is due

Table 2. Selected bond distances (Å) and angles (°) of 1.

Bond distances (Å)			
Mn-Cl1	2.3445(9)	N1-C7	1.471(3)
Mn-Cl2	2.4069(8)	N1-C13	1.494(4)
Mn-N1	2.571(2)	N2-N3	1.375(3)
Mn-N2	2.170(2)	N2-C4	1.337(4)
Mn-N4	2.197(3)	N4-N5	1.375(3)
N1-C1	1.454(3)	N4-C8	1.339(4)
Bond angles (°)			
Cl1-Mn-Cl2	108.64(3)	N2-Mn-N4	138.47(9)
Cl1-Mn-N1	161.24(5)	Mn-N1-C1	98.89(15)
Cl1-Mn-N2	108.55(6)	Mn-N1-C7	95.03(13)
Cl1-Mn-N4	103.05(6)	Mn-N1-C13	126.70(16)
Cl2-Mn-N1	89.94(5)	Mn-N2-N3	117.06(17)
Cl2-Mn-N2	96.95(6)	Mn-N2-C4	137.74(19)
Cl2-Mn-N4	97.78(6)	Mn-N4-N5	113.83(17)
N1-Mn-N2	70.53(8)	Mn-N4-C8	141.30(18)
N1-Mn-N4	70.88(8)		
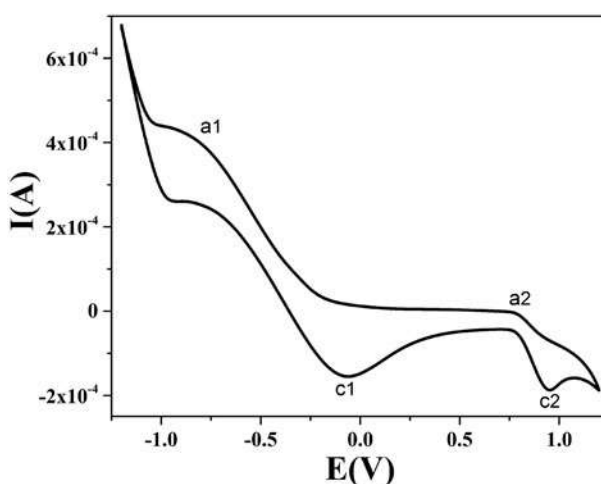
Figure 4. Cyclic voltammogram of 1 in methanol containing tetrabutylammonium perchlorate as the supporting electrolyte at a scan rate of 100 mV s^{-1}.

to relieving some of the steric stains arising out of the bulky napthyl group and two methyl groups in the 3- and 5-position of pyrazole ring. Similar results in bond parameters were also observed in literature [42–46]. The weak interaction between Mn and N1 gives lability in the structure of coordination, which may impart the property to bind with molecular oxygen. Selected bond distances and angles of complex are given in Table 2. The remaining bond lengths and angles of **1** are listed in Supplementary Table S1. The ORTEP diagrams of **2–5** are given in Supplementary Figures S2–S5 to know the appropriate structure of the molecules.

3.4. Electrochemical study

Electrochemical study of **1** is performed using methanol as solution and tetrabutylammonium perchlorate as supporting electrolyte at scan rate 100 mV/sec in the potential

range $+1.0$ V to -1.0 V. As shown in Figure 4, **1** shows only the reductive response at -0.89 V in cathodic scan while two oxidative waves appear at $+0.95$ V and $+0.087$ V. The reductive wave at -0.89 V corresponds to oxidative wave $+0.087$ V; this oxidation and reduction couple corresponds to a quasi-reversible redox process of Mn(III)/Mn(II) couple [43, 44]. The average formal potential $E_{1/2} = -0.48$ V. The other oxidation wave at $+0.95$ V has no corresponding counterpart in the cathodic wave, practically $I_P = 0$ for the potential range to $+0.75$ V, indicating the absence of electroactive species in forward scan. The $(I_P)_a$ value -2×10^{-4} A at $+0.95$ V may be due to the formation of manganese(II) oxide. The sequence of redox process can be presented as:

$$Mn^{III} \rightleftharpoons Mn^{II} \rightleftharpoons Mn$$

The details of peak potential values and $E_{1/2}$ values for the complex are listed in Table 3.

3.5. Phenoxazinone synthase (PHS) and catechol oxidase (CO) activity

Phenoxazinone synthase is a multicopper oxidase enzyme which catalyzes the biosynthesis of the actinomycin D by streptomycin antibiotics. The catalysis reaction is concerned with the oxidative condensation of two molecules of 3-hydroxo-4-methyl-anthranilic acid pentapeptide lactone to form phenoxazinone chromophore. In biomimetic chemistry, enzymes PHS and CO have been widely attempted for modeling the active sites not only using copper(II) complexes [47] but also with several manganese [43, 44, 46] and cobalt [42, 45] complexes with redox behavior. Manganese might be the best alternative metal for performing PHS and CO activity other than nature's choice copper [23]. Comparison showed that Mn^{II} complexes of N,O-donors showed better PHS and CO activity than Co^{II} and Cu^{II} analogues [23]. In the present report, we model manganese, copper, and cobalt complexes to compare their k_{cat} values. Figure 5 shows the UV-vis spectra for the oxidation OAPH (concentration 1×10^{-2} M) catalyzed by **1**, **3,** and **4** (1×10^{-5} M) and oxidation of 3,5-ditertiary-butylcatechol (1.0×10^{-2} M) catalyzed by **3** and **4** up to 2 h of reaction in oxygenated methanol at 25 °C. Supplementary Figure S6 shows the UV-vis spectra for the oxidation of OAPH by **2** and **5** at similar conditions.

To know the extent of the catalytic efficiency of the complexes, kinetic studies are performed. For this purpose, a 1×10^{-5} M solution of **1–5** is allowed to react with about 10-fold concentrated OAPH solution to meet a pseudo-first-order rate law. All the experiments are performed at 25 °C under aerobic conditions. The initial rate of reaction of **1–5** shows rate saturation kinetics as shown in Supplementary Figure S7. This observation indicates the formation of substrate-catalyst intermediate and the rate-determining step is the decomposition step of the intermediate. Michaelis–Menten enzymatic kinetics is used to understand the kinetics of PHS [48]. The observed and simulated initial rates *versus* substrate concentrations of the non-linear plot and the Lineweaver–Burk plot for **1–5** are shown in Supplementary Figure S8. The value of Michaelis binding constant (K_m) and V_{max}, and the turnover number (K_{cat}) of the complexes, are listed in Table 4. A linear relationship for the initial rates is obtained varying the complex concentration which gives first-order reaction kinetics.

Table 3. Cyclic voltammetry data for **1–5**.

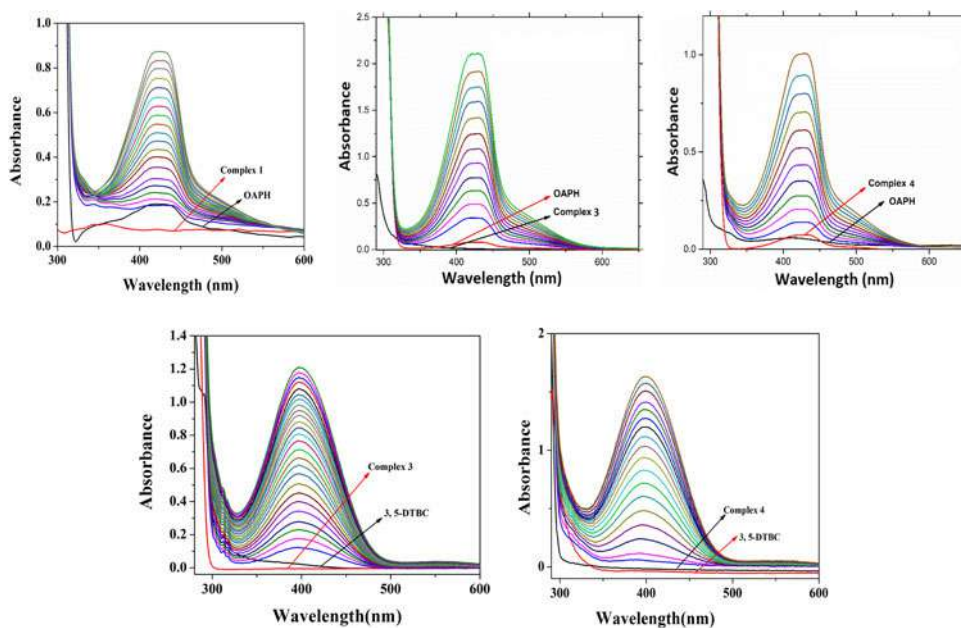| Complex	E_{pa1}	E_{pc1}	$(E_{1/2})_1$	E_{pa2}	E_{pc2}	$(E_{1/2})_2$
1	−0.89	−0.08	−0.48	0.76	0.95	0.85
2	1.36	1.71	1.536	–	–	–
3	0.38	0.55	0.46	0.75	0.93	0.84
4	0.38	0.49	0.43	0.77	0.93	0.85
5	0.79	0.91	0.90	–	–	–

Figure 5. The time resolved spectral profile showing oxidation of *o*-aminophenol (1.0×10^{-2} M) catalyzed by **1**, **3** and **4** and 3,5-ditertiary-butylcatechol (1.0×10^{-2} M) catalyzed by **3** and **4** in dioxygen-saturated methanol. The spectra were recorded at 5 min intervals under aerobic conditions at room temperature.

As shown in Table 4, the turnover number (K_{cat}) for the oxidation of OAPH follows the order **3** > **4** > **5** > **1** > **2**. The higher reactivity of **3** and **4** is due to the dinuclearity in the molecule, which confirms stable binding with molecular O_2 in the labile copper centers of the complex. Relatively lower K_{cat} values of mononuclear complexes **1**, **2,** and **5** than dinuclear **3** and **4** are probably due to steric crowding arising from the napthyl/pyridine group around the metal center of **1**, **2,** and **5** (ORTEP of **2** and **5** in Supplementary Figures S4 and S5). The steric effect resists the oxygen binding to the metal center. However, the same steric effect somehow is less in the dinuclear complex (ORTEP of **3** and **4** in Supplementary Figures S2 and S3) as the metal centers are sufficiently separated by bridged bonds. The greater the steric repulsion in the system, the lesser is the formation of substrate binding property.

Complexes **3** and **4** show higher catecholase activity than recently reported compounds bearing similar scaffolds [24, 25]. A tentative catalytic cycle can be proposed based on the kinetics. The OAPH forms an adduct with the metal complex in the first step. The adduct yields aminophenol radical in the reaction with dioxygen, which is rate-determining step for the process. The OAP radical generates ortho-benzoquinone

Table 4. Kinetic parameters of phenoxazinone synthase activity of **1–5** and catecholase activity of 3 and 4.

Substrate	Catalyst	V_{max} (Ms^{-1})	K_M (M)	k_{cat} (h^{-1})
OAPH	1	4.211×10^{-8}	1.68×10^{-3}	15.15
	2	1.51×10^{-8}	1.56×10^{-3}	5.45
	3	$(1.48 \pm 0.01) \times 10^{-7}$	$(1.55 \pm 0.6) \times 10^{-3}$	53.28
	4	$(1.05 \pm 0.06) \times 10^{-7}$	$(5.58 \pm 0.6) \times 10^{-3}$	37.80
	5	5.65×10^{-8}	1.01×10^{-3}	20.36
3,5-DTBC	3	7.89×10^{-8}	6.35×10^{-3}	28.40
	4	1.12×10^{-7}	1.33×10^{-3}	40.24

monoamine [48–51]. Representative CO activities of **3** and **4** are also performed using substrate 3,5-di*tert*-butyl catechol (3,5-DTBC). 3,5-DTBC has two bulky methyl groups in the ring with low reduction value for quinone-catechol transformation. Upon treatment of methanolic solution of **3** and **4** into 100 equivalents of 3,5-DTBC in aerobic condition, repetitive spectra were recorded (Figure 5). The colorless 3,5-DTBC solution turns into deep brown, indicating the conversion of 3,5-DTBC to corresponding quinone.

The smooth increases of quinone band around 390 nm which shifts ultimately to 401 nm. The same reaction is carried out at a substrate catalyst concentration 1×10^{-5} M. The time-dependent change in absorption at a wavelength of 401 nm was measured for 25-min interval to find out the reaction rate. The difference of absorption (ΔA) at 401 nm is plotted against time to get the rate/velocity for that particular catalyst to substrate concentration ratio. The reaction kinetics were studied by observing the time-dependent change in absorption at a wavelength of 401 nm for catalysis in methanol. The ΔA *versus* time plot gives the rate of the reaction. First-order reaction kinetics with rate 6.35×10^{-3} min^{-1} and 1.33×10^{-3} min^{-1} in methanol are observed for **3** and **4**, respectively (Supplementary Figure S7). The rate of each concentration of the substrate was determined by the initial rate method. The rate *versus* concentration of the substrate plots are analyzed on the basis of Michaelis–Menten approach of enzymatic kinetics to obtain the Lineweaver–Burke (double reciprocal) plot as well as the values of the various kinetic parameters (V_{max}, K_m, and K_{cat}). The observed rate *versus* substrate concentration plot as well as Lineweaver–Burke plot in methanol are given in Supplementary Figures S7 and S8, respectively. The kinetic parameters are listed in Table 4. From the results of kinetic study, a mechanism is proposed for CO. The process may follow two step mechanistic pathways. The first step is the rate-determining step where probably 1:1 adduct of catalyst-substrate is formed [52–57].

3.6. Antimicrobial activities

The ability to penetrate the cell wall of a foreign compound determines the extent of antimicrobial activity. The antibacterial/antifungal agents target the structures and functions or both which are relevant to the inhibitory activity of the organisms. The structural types with the combination of pyridyl/napthalene group in the pyrazole moiety might have high effect on biological potency by regulating the lipid-water partition coefficient and binding affinity to target enzymes. The results in the present *in vitro* antimicrobial activities and MIC values of L^1, L^2 and **1–5** are presented in Table 5

Table 5. Antimicrobial activity of specific concentration (1000 µg/mL) of different synthetic metal complex compared with control by agar well diffusion method.

	Zone of inhibition (cm) against bacteria and fungi (Mean ± SD)									
	Gram-positive bacteria			Gram-negative bacteria					Fungi		
Sample	S. aureus	S. faecalis	B. subtilis	K. pneumonia	P. vulgaris	E. coli	P. aeruginosa	S. typhi	A. flavus	C. albicans
1	2.5 ± 0.01	1.7 ± 0.05	1.5 ± 0.05	1.1 ± 0.01	1.1 ± 0.01	1.8 ± 0.01	1.3 ± 0.01	0.9 ± 0.01	1.9 ± 0.01	2.1 ± 0.01
2	2.0 ± 0.05	1.1 ± 0.05	1.3 ± 0.06	1.1 ± 0.01	1.0 ± 0.01	1.4 ± 0.05	1.1 ± 0.01	1.1 ± 0.01	1.4 ± 0.01	1.9 ± 0.01
3	0.9 ± 0.05	1.6 ± 0.05	1.3 ± 0.05	0.9 ± 0.05	1.4 ± 0.05	1.7 ± 0.01	1.8 ± 0.01	1.3 ± 0.01	1.6 ± 0.01	2.7 ± 0.05
4	0.9 ± 0.05	1.1 ± 0.05	1.3 ± 0.01	0.9 ± 0.01	1.4 ± 0.01	1.2 ± 0.03	1.4 ± 0.05	1.3 ± 0.05	1.7 ± 0.05	2.0 ± 0.05
5	1.3 ± 0.05	1.6 ± 0.01	1.1 ± 0.01	0.9 ± 0.02	1.0 ± 0.01	1.1 ± 0.01	0.9 ± 0.02	0.9 ± 0.01	1.2 ± 0.01	1.4 ± 0.05
L[1]	1.6 ± 0.02	1.6 ± 0.02	1.7 ± 0.02	0.9 ± 0.01	1.5 ± 0.01	1.8 ± 0.05	0.9 ± 0.05	1.6 ± 0.03	2.0 ± 0.05	2.4 ± 0.01
L[2]	2.1 ± 0.01	0.9 ± 0.01	1.8 ± 0.05	0.9 ± 0.02	1.5 ± 0.02	1.7 ± 0.05	0.9 ± 0.05	1.4 ± 0.02	1.7 ± 0.01	2.4 ± 0.05
Control										
MeCN	0.9 ± 0.06	0.9 ± 0.05	1.0 ± 0.01	0.9 ± 0.05	1.1 ± 0.05	1.2 ± 0.01	0.9 ± 0.05	1.0 ± 0.05	1.1 ± 0.05	1.0 ± 0.01
DMSO	0.9 ± 0.06	1.2 ± 0.05	1.0 ± 0.01	0.9 ± 0.05	1.0 ± 0.05	1.0 ± 0.02	0.9 ± 0.05	1.1 ± 0.05	1.2 ± 0.05	1.0 ± 0.01

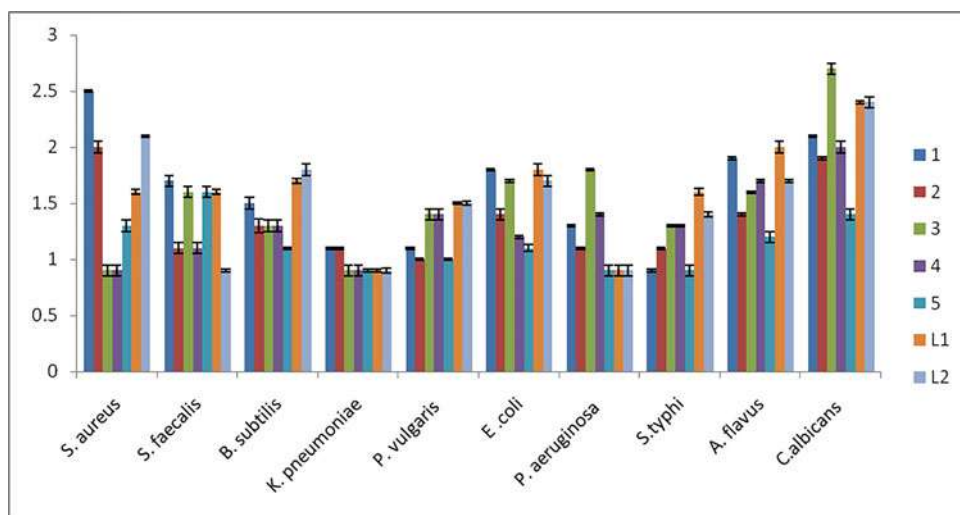MeCN: acetonitrile; DMSO: dimethyl sulfoxide.

Figure 6. Graphical presentation of sensitivity of the compounds against different bacteria and fungi.

Table 6. The lipophilicity values of ligands and their corresponding metal complexes in logarithm form.

Sample ID	Water		1-Octanol		P	logP
	Concentration (M)	Absorbance	Concentration (M)	Absorbance		
1	4.509×10^{-4}	0.19952	2.296×10^{-3}	1.0159	5.092	0.7068
2	1.751×10^{-3}	0.3335	7.59×10^{-3}	1.5159	4.334	0.6369
3	1.735×10^{-3}	1.2423	3.547×10^{-3}	2.5399	2.0443	0.3105
4	1.687×10^{-3}	1.238	3.407×10^{-3}	2.4996	2.0195	0.3052
5	4.983×10^{-3}	2.6140	5.9445×10^{-3}	3.1179	1.1929	0.0766
L^1	2.073×10^{-3}	0.8484	4.285×10^{-3}	1.7539	2.067	0.315
L^2	1.84×10^{-3}	0.2215	4.141×10^{-3}	0.49833	2.250	0.352

and Supplementary Table S2, respectively. The sensitivity of these compounds against different bacteria and fungi is graphically represented in Figure 6. The sensitivity and MIC values of some standard antibiotics are given in Supplementary Tables S3–S6 to compare the activity that is shown by the compounds under investigation. The camera views of the sensitivity of tested bacteria and fungi against the present compounds are shown in Supplementary Figures S9 and S10. The present study reveals that L^1 and L^2 show better antibacterial activity than their metal complexes. This may be explained in terms of high structural strain in L^1 and L^2 (Figure 1) arising from the presence of two and one bulky group of N-(methyl-3,5-dimethyl-pyrazole), respectively. The presence of three bulky groups in the aliphatic tertiary N-atom registers high strain to the ligand structures which can disrupt the cell division/DNA replication of the bacteria (prokaryotes). The general order of antibacterial activity is found as L^1 > L^2 > **1** > **3** > **2** > **4** > **5**. Among the complexes, **1** shows excellent antibacterial activity against *E. coli*, *S. aureus*, *S. faecalis* and *Bacillus sp* with MIC values 300, 200, 400 and 300 μg/mL, respectively, whereas **3** also has comparable antibacterial activities against *P. aeruginosa*, *S. faecalis* and *P. vulgaris* with MIC values of 400, 600 and 300 μg/mL, respectively. Therefore, L^1, L^2, **1** and **3** can be regarded as significant

antibacterial agents for environmental cleanup and also can be used as drug. The present order of antibacterial activity of the metal complexes may be attributed to the inhibition of the synthesis of the peptidoglycan layer of bacterial cell walls.

All the ligands and the complexes show good antifungal activities against eukaryotes *A. flavus* and *C. albicans*. The antifungal screening data typically show the reverse order of antibacterial activity, i.e. the metal complexes have a greater inhibitory tendency than the free ligands. Among the complexes, the antifungal activity order is found as manganese(II)-complex, d^5 ($t_{2g}^5 e_g^0$) (**1**) > copper(II)-complex, d^9 ($t_{2g}^6 e_g^3$) (**3** and **4**) > cobalt(II)-complex, d^7 ($t_{2g}^6 e_g^1$) (**2** and **5**). In this context, the increased activity of the metal complexes can be explained in terms of lability and lipophilicity. The d^5 to d^9 systems are generally labile with e_g filling of electron(s) with respect to ligand substitution reaction leading to formation of metal-DNA adduct. Metal ions having unpaired electron (one unpaired electron in each case) are highly polar in nature. The chelation phenomenon minimizes the polarity of the metal ion due to potential charge sharing between metal and donors, and subsequently increases the lipophilic character of the metal complex. The logP values are presented in Table 6. The higher lipophilicity of the compounds accelerates the cell permeation, leading to cell damage. It can be concluded that the antifungal activity of the complex increases with the increased lipophilicity.

4. Conclusion

Napthyl-anchored pyrazole ligand with multiple nitrogen donor atoms produce monomeric complexes of manganese(II) (**1**) with distorted square pyramidal structure. The monomeric complexes of napthyl/pyridyl-anchored pyrazole ligand are moderately reactive towards the catalytic oxidation of o-amino-phenol whereas dimeric Cu^{II} complexes are very effective models of phenoxazinone synthase and catecholase activities. The catalytic efficiency mainly arises from the structural aspects of the crowded pyrazole derived compounds. The highly-crowded complexes (**1**, **2** and **5**) show less catalytic promiscuity than less-crowded bridged copper(II) complexes (**3** and **4**). Most of the reported compounds have the property to destroy the cell of pathogen bacteria and fungi. Ligands are good antibacterial agents where metal complexes are capable in showing better antifungal activity than the ligands. There is a scope to explore in the structure-activity relationship with pyrazole-based lead compounds for biological applications.

Disclosure statement

There is no conflict of interest to declare.

Funding

ORCID

Paula Brandão http://orcid.org/0000-0002-4746-6073
Pulakesh Bera http://orcid.org/0000-0001-8566-0742

References

[1]   N.M. Abunada, H.M. Hassaneen, N.G. Kandile, O.A. Miqdad. *Molecules*, **13**, 1501 (2008).
[2]   A.B. Adnan, T.A. Aziem. *Bioorg. Med. Chem.*, **12**, 1935 (2004).
[3]   E. Aiello, S. Aiello, F. Mingoia, A. Bacchi, G. Pelizzi, C. Musiu, M.G. Setzu, A. Pani, P.L. Colla, M.E. Marongiu. *Bioorg. Med. Chem.*, **8**, 2719 (2000).
[4]   E. Akbas, I. Berber. *Eur. J. Med. Chem.*, **40**, 401 (2005).
[5]   J. Parez, L. Liera. *Eur. J. Inorg. Chem.*, **33**, 4913 (2009).
[6]   J.S. Larsen, M.A. Zahran, E.B. Pedersen, C. Nielsen. *Monatsh. Chem.*, **130**, 1167 (1999).
[7]   I. Bouabdallah, L.A. M'Barek, A. Zyad, A. Ramdani, I. Zidane, A. Melhaoui. *Nat. Prod. Res.*, **20**, 1024 (2006).
[8]   H.J. Park, K. Lee, S. Park, B. Ahn, J.C. Lee, H.Y. Cho, K.I. Lee. *Bioorg. Med. Chem. Lett.*, **15**, 3307 (2005).
[9]   A.H. Abadi, A.A.H. Eissa, G.S. Hassan. *Chem. Pharm. Bull.*, **51**, 838 (2003).
[10] M.K. Sharma, P.R. Murumkar, A.M. Kanhed, R. Giridha, M.R. Yadav. *Eur. J. Med. Chem.*, **79**, 298 (2014).
[11] M. Ezawa, D.S. Garvey, D.R. Janero, S.P. Khanapure, L.G. Letts, A. Martino, R.R. Ranatunge, D.J. Schwalb, D.V. Young. *Lett. Drug Des. Discov.*, **2**, 40 (2005).
[12] A. Mishra, A.K. Tewari. *Bioorg. Med. Chem.*, **9**, 715 (2001).
[13] I.V. Mashevskaya, S.V. Kol'tsova, E.V. Voronina, T.F. Odegova, A.N. Maslivets. *Pharm. Chem. J.*, **35**, 18 (2001).
[14] V. Michon, C.H. Du Penhoat, F. Tombret, J.M. Gillardin, F. Lepage, L. Berthon. *Eur. J. Med. Chem.*, **30**, 147 (1995).
[15] I. Yildirim, N. Özdemir, Y. Akçamur, M. Dinçer, O. Andaç. *Acta Cryst. E*, **61**, 256 (2005).
[16] D.M. Bailey, P.E. Hansen, A.G. Hlavac, E.R. Baizman, J. Pearl, A.F. Defelice, M.E. Feigenson. *J. Med. Chem.*, **28**, 256 (1985).
[17] C.K. Chu, J. Cutler. *J. Heterocycl. Chem.*, **23**, 289 (1986).
[18] E.I. Solomon, D.E. Heppner, E.M. Johnston, J.W. Ginsbach, J. Cirera, M. Qayyum, M.T. Kieber-Emmons, C.H. Kjaergaard, R.G. Hadt, L. Tian. *Chem. Rev.*, **114**, 3659 (2014).
[19] J. Kaizer, G. Barath, R. Csonka, G. Speier, L. Korecz, A. Rockenbauer, L. Parkanyi. *J. Inorg. Biochem.*, **102**, 773 (2008).
[20] G. Blay, I. Fernández, J.R. Pedro, R. Ruiz-García, T. Temporal-Sánchez, E. Pardo, F. Lloret, M.C. Muñoz. *J. Mol. Catal. A: Chem.*, **250**, 20 (2006).
[21] S.D. Copley. *Curr. Opin. Chem. Biol.*, **7**, 265 (2003).
[22] I.A. Koval, P. Gamez, C. Belle, K. Selmeczi, J. Reedijk. *Chem. Soc. Rev.*, **35**, 814 (2006).
[23] S.K. Dey, A. Mukherjee. *Coord. Chem. Rev.*, **310**, 80 (2016).
[24] I. Bouabdallah, R. Touzani, I. Zidane, A. Ramdani. *Catal. Commun.*, **8**, 707 (2007).
[25] N. Boussalah, R. Touzani, I. Bouabdallah, S. El Kadiri, S. Ghalem. *J. Mol. Catal. A: Chem.*, **306**, 113 (2009).
[26] M.R. Malachowski, M.G. Davidson. *Inorg. Chim. Acta*, **162**, 199 (1989).
[27] I. Banerjee, J. Marek, R. Herchel, M. Ali. *Polyhedron*, **29**, 1201 (2010).
[28] A. Jana, P. Brandão, G. Mondal, P. Bera, A. Santra, A.D. Jana, R.B. Mokhamatam, S.K. Manna, N. Bhattacharyya, P. Bera. *Inorg. Chim. Acta*, **482**, 621 (2018).
[29] A. Santra, G. Mondal, M. Acharjya, P. Bera, A. Panja, T.K. Mandal, P. Mitra, P. Bera. *Polyhedron*, **113**, 5 (2016).
[30] A.D. Becke. *J. Chem. Phys.*, **98**, 5648 (1993).
[31] R.G. Parr, W. Yang. *Density Functional Theory of Atoms and Molecules*, Oxford University Press, Oxford (1989).

[32] C. Lee, W. Yang, R.G. Parr. *Phys. Rev. B Condens. Matter*, **37**, 785 (1988).
[33] Bruker. *SAINT (Version 6.28a) and SADABS (Version 2.03): Data Reduction and Absorption Correction Program*, Bruker AXS Inc., Madison, WI (2001).
[34] Bruker. *SMART (Version 5.625): Data Collection Program*, Bruker AXS Inc., Madison, WI (2001).
[35] G.M. Sheldrick. *SHELXL-97, Crystal Structure Refinement Program*, University of Göttingen, Germany (1997).
[36] B. Kupcewicz, M. Ciolkowski, B.T. Karwowski, M. Rozalski, U. Krajewska, I.P. Lorenz, P. Mayer, E. Budzisz. *J. Mol. Struct.*, **1052**, 32 (2013).
[37] D.A. van den Berghe, A.J. Vlietinck. In *Methods in Plant Biochemistry*, P.M. Dey, J.B. Harbone (Eds.), p. 47, Academic Press, London (1991).
[38] A. Nostro, M.P. Germanò, V. D'Angelo, A. Marino, M.A. Cannatelli. *Lett. Appl. Microbiol.*, **30**, 379 (2000).
[39] A. Jana, M. Dolai, B.K. Shaw, S.K. Saha, M. Ali. *Transition Met. Chem.*, **3**, 347 (2016).
[40] A. Solanki, M. Monfort, S.B. Kumar. *J. Mol. Struct.*, **1050**, 197 (2013).
[41] A.W. Addison, T.N. Rao, J. Reedijk, J. van Rijn, G.C. Verschoor. *J. Chem. Soc., Dalton Trans.*, 1349 (1984).
[42] A. Panja. *Dalton Trans.*, **43**, 7760 (2014).
[43] A. Panja. *RSC Adv.*, **4**, 37085 (2014).
[44] A. Panja. *Polyhedron*, **79**, 258 (2014).
[45] A. Panja, M. Shyamal, A. Saha, T.K. Mandal. *Dalton Trans.*, **43**, 5443 (2014).
[46] A. Panja, N.C. Jana, S. Adak, K. Pramanik. *Inorg. Chim. Acta*, **459**, 113 (2017).
[47] M.R. Maurya, S. Sikarwar, T. Joseph, S.B. Halligudi. *J. Mol. Catal. A: Chem.*, **236**, 132 (2005).
[48] A.J. Kenneth, S.G. Roger. *Biochemistry*, **50**, 8264 (2011).
[49] T. Horvath, J. Kaizer, G. Speier. *J. Mol. Catal. A: Chem.*, **215**, 9 (2004).
[50] L.I. Simandi, T. Barna, S. Nemeth. *J. Chem. Soc., Dalton Trans.*, 473 (1996).
[51] T.M. Simandi, Z. May, I.C. Szigyarto, L.I. Simandi. *Dalton Trans.*, 365 (2005).
[52] A. Martínez, I. Membrillo, V.M. Ugalde-Saldívar, L. Gasque. *J. Phys. Chem. B*, **116**, 8038 (2012).
[53] A. Banerjee, R. Singh, E. Colacio, K.K. Rajak. *Eur. J. Inorg. Chem.*, **2009**, 277 (2009).
[54] L. Gasque, V.M. Ugalde-Saldívar, I. Membrillo, J. Olguín, E. Mijangos, S. Bernès, I. González. *J. Inorg. Biochem.*, **102**, 1227 (2008).
[55] M. Merkel, N. Möller, M. Piacenza, S. Grimme, A. Rompel, B. Krebs. *Chemistry*, **11**, 1201 (2005).
[56] I.A. Koval, C. Belle, K. Selmeczi, C. Philouze, E. Saint-Aman, A.M. Schuitema, P. Gamez, J.-L. Pierre, J. Reedijk. *J. Biol. Inorg. Chem.*, **10**, 739 (2005).
[57] T. Mallat, A. Baiker. *Chem. Rev.*, **104**, 3037 (2004).